Contents lists available at ScienceDirect

Optics and Lasers in Engineering

Appearance evaluation of digital materials in material jetting

Ali Payami Golhin*, Are Strandlie

Department of Manufacturing and Civil Engineering, NTNU - Norwegian University of Science and Technology, Gjøvik, 2815 Norway

ABSTRACT

Material jetting (MJT) products have a high subjective appearance quality in additive manufacturing (AM). MJT objects are typically manufactured from multiple layers of semi-transparent photo resins to achieve the desired appearance. This study explores the optical properties of photopolymer plates in monolayer and bilayer combinations. The role of the white substrate as the background plate in bilayer configurations is discussed concerning appearance reproduction in MJT parts. For this purpose, spectral reflectance, transmittance, absorbance, color difference, and texture were investigated for MJT objects with different plate combinations. The primary digital materials in MJT were further investigated for haze, gloss, scattering variations, and their corresponding bidirectional reflectance distribution functions (BRDFs). The optical properties of the studied surfaces were then applied to three-dimensional (3D) models to illustrate the variation in visual appearance and texture. According to the results, it was inevitable to use a white background plate for color reproduction. Therefore, increasing the layer thickness did not improve color fidelity. Due to the role of microfacet normals in the surface texture, gloss, haze, and scattering, results followed the same analysis pattern but depended on the measurement direction.

1. Introduction

MJT[1], including the PolyJet®, is an AM[2] technique that promotes multi-material 3D printing, utilizing UV[3]-curable polymer inks. In terms of full-appearance reproduction, MJT is one of the main AM categories. 3D printers with PolyJet technology are ideal for depositing tiny droplets of material with different appearances into voxels following the design. MJT machines can print fine details and achieve a consistent surface finish using a PolyJet 3DP process with little to no visible layering [1]. Unlike conventional printers, MJT models can represent relatively smooth, glossy surfaces with consistent colors since the materials are mixed in the same layer but with different color cartridges.

The MJT printers are able to mix and match colors since each droplet of material contains its own mini pool of ink. The flow of fluid in pools can affect the appearance and shape of structured layers, as seen previously in high-temperature process methods, such as the welding process [2–4]. This allows designers to have a great deal of flexibility regarding the appearance of their products. Thus, the MJT is ideally suited to applications in which appearance is essential for consumer goods, such as medical models [5] or jewelry [6]. However, the movement of the printhead, i.e., nozzles, and build platform, affects the shape and combination of the voxels, resulting in variations in the appearance [7,8]. The

design of a 3D object, along with multiple printer parameters, must be carefully controlled to achieve high-fidelity reproductions of both the shape and appearance of the 3D object [8,9]. Aside from this, optical metrology systems are closely related to similarity evaluations of topography measurements in additive manufacturing [10], which depend on the design of the parts.

Since the optical properties of an object determine its visual quality, industries are concerned about the appearance of their products. Furthermore, customers expect uniformity when dealing with groups of the same product. As a result of observing the differences between similar products, consumers commonly attribute the inferior quality [11]. As Yuan [8] described, color reproduction can be divided into four categories: colorimetric difference assessment, computer-aided colorization, optical parametric modeling, and droplet jetting. Based on Pointer [12], total appearance can be described as size, shape, gloss, texture, and other visual characteristics.

In order to reach the high appearance fidelity of the 3D-printed part with the designed model, several characteristics that contribute to the optical properties of objects should be studied, including color, gloss, texture, translucency, haze, and subsurface scattering [13,14]. Texture mapping is essential to the reproduction of an appearance using AM. This process involves applying an image texture to a 3D surface to create the appearance of a real surface [15,16]. For this purpose, a list of vertex-to-UV coordinate mappings is included in the 3D model when a 3D object with texture mapping is imported [17]. Texture mapping provides several advantages for measurement, including accurate representation, increased detail, and rapid and non-destructive measurement [18]. It can be used in a wide range of measurement applications, ranging from engineering and manufacturing [19] to preserving cultural

* Corresponding author.
E-mail address: ali.p.golhin@ntnu.no (A.P. Golhin).
[1] Material jetting
[2] Additive manufacturing
[3] Ultraviolet

heritage and restoring art [20]. Although limited research has been conducted on the appearance of MJT parts [8,21-24], the study of these various attributes simultaneously is lacking in the literature.

As we discussed in our previous works [8,25,26], the MJT object should be manufactured in a bilayer structure (overlay of two plates) to achieve optimal color reproduction. The influence of bilayer structure on MJT 3D printing, however, was not studied. Bilayer structures have been used in advanced manufacturing in a variety of aspects, including functional and optical properties. A review by Hong et al. [27] examined structural color materials and their applications in optical encryption and anticounterfeiting, in particular bilayer structures. Nam et al. [28] addressed full-color woodpile photonic crystals via interference from a conformal multilevel phase mask based on bilayer structures. Using different polymer and composite abutments, Hsu et al. [29] evaluated the color accuracy of multilayer pre-colored zirconia polycrystal dental prostheses. Egorov et al. [30] compared 3D printing with simple bilayer objects using fused deposition modeling (FDM) and stereolithography (SLA) methods for electrochemical energy storage. However, these works were limited to the functional and only color-appearance attributes of the bilayer structures. Accordingly, no studies discussed the significance of the white plate of the bilayer objects in appearance, particularly for non-color attributes and in rotational MJT.

This study provides insight into the appearance and texture mapping of structured surfaces manufactured using PolyJet technology. The role of bilayer structure using a white background in MJT technology is examined for the first time concerning appearance reproduction using various optical attributes. For this purpose, this work includes studies on color, gloss, translucency, texture, haze, scattering, and BRDFs[4] for printed plates with different thicknesses and color combinations. It is described how the appearance of 3D printing, as a unique approach to additive manufacturing, interacts with the hard proofing and quality improvement of AM surfaces.

2. Materials and methods

2.1. Material jetting

A Stratasys J55 PolyJet material jetting machine was used to 3D print the polymeric coupons, which were made of VeroCyan (RGD843), VeroBlackPlus (RGD875), VeroYellow (RGD836), VeroMagenta (RGD851), and VeroPureWhite (RGD837) photo-resins. The standard tray material was applied to the 3D models imported to the Stratasys GrabCAD Print software. In this paper, the terms "cyan", "magenta", "yellow", "black", and "white" have been used to designate the colors of coupons. Vero materials offer low viscosity acrylic oligomers mixed with exo-1,7,7-trimethylbicyclo[2,2,1]hept-2-yl acrylate, (octahydro-4,7methano-1H-indenediyl) bis(methylene) diacrylate, and 4-(1-oxopropenyl)-morpholine [31]. Vero photo-resins share similar material properties, including mechanical, thermal, and electrical characteristics [32].

As shown in Fig. 1, the role of the white color background was studied using three sets of specimens. The monolayer (plate) of cyan, magenta, yellow, black, and white (CMYKW) photo resins were manufactured at various thicknesses (1.00 ± 0.02 mm and 2.00 ± 0.02 mm), hereafter referred to as 1 mm and 2 mm samples. Bilayer structures were built using 1 mm plates of each CMYKW color separately with a white background of 1 mm thickness. The size of the specimens was 35.50 ± 0.50 mm (width) $\times$ 40.00 ± 0.50 mm (length), fabricated on the middle swath of a rotary disc as the build platform with a glossy-on-glossy surface finish. The process was followed by support removal using a waterjet system. Five measurements from two sets of specimens were collected for each for reproducibility in measuring appearance.

2.2. Appearance study

Spectrophotometry was conducted using a UV/Vis/NIR Spectrometer (PerkinElmer Lambda 1050+) equipped with the 3-detector module in an integrating sphere configuration (150 mm) with a wavelength accuracy of 1 nm. The reflectance, specular transmission, and absorbance spectra of photopolymer plates in the wavelength range 200-2000 nm and sampling interval of 5 nm were recorded with the specimens aligned regarding the detector window. Spectral reflectance results were collected in the visible range of 380 to 780 nm for color evaluation. To minimize the effect of layer-by-layer inhomogeneity and the edge effect resulting from light scattering, the largest possible area in the middle of the specimens was exposed to a light beam. Thus, the measurement area was limited to the size of the transmittance (25 mm $\times$ 16 mm) and reflectance (24 mm in diameter) ports (Fig. 2).

The computational color science toolbox in MATLAB R2022a [33] was used to calculate colorimetric values. A color-matching function derived from ASTM E308-01 [24] and designed by the International Commission on Illumination (CIE[5]) was used to calculate CIEXYZ tristimulus values. The CIE 2° color matching functions and the D50 illuminant were used to determine tristimulus values. As a result, CIEL*a*b* coordinates were further determined according to CIE1976. CIEL*a*b* and CIEL*C*h* color spaces define colors based on three coordinates for each, where L* is the lightness, a* and b* stand for the red-green and blue-yellow axes, C* corresponds to chroma, and h* relates to hue angle. Colorimetric differences of 1 mm and 2 mm sample types were compared with bilayer samples using CIEDE2000 color difference according to the following equation

$$CIEDE2000 = \sqrt{\left(\frac{\Delta L^*}{k_L S_L}\right)^2 + \left(\frac{\Delta C^*}{k_c S_C}\right)^2 + \left(\frac{\Delta h^*}{k_h S_h}\right)^2 + R_T f(\Delta C^* \Delta h^*)} \tag{1}$$

where ΔL^* (lightness), ΔC^* (chroma) and Δh^*(hue) represent their variant due to the color change, and the R_T variable consists of the hue rotation term. S_L, S_C, and S_h correspond to CIEL*C*h* lightness compensation, and k_L, k_C, and k_h constants were set to the unit value. The color space is designed to be perceptually uniform, meaning that the same amount of distance between two points corresponds to roughly the same amount of perceived color difference. As a result, they can be used for comparing color differences and specifying colors across different media and devices.

To assess the color difference among CMYKW plates with different thicknesses and their corresponding bilayer reference spectra, the MCDM[6] and the RMSE[7] were determined as

$$MCDM = \frac{1}{N} \sum_{i=1}^{N} \Delta E(C_i, C_m) \tag{2}$$

$$RMSE = \sqrt{\frac{1}{N} \sum_{i=1}^{N} (r_{r,i} - r_{t,i})^2} \tag{3}$$

where N is the number of results, r_t and r_r relate to the spectral results of tests and references, C_i implies the color coordinate of the ith measurements, and C_m is the reflectance average.

To assess the texture, the xTex scanner by Vizoo was used, and the 3D texture models were rendered using Blender 2.79 engine. For this purpose, collected surface maps, including alpha, base, displacement, material, surface normal, and roughness, were imported as texture data. Using a light-controlled Lightbox, multiple photos were taken of a sample under varying lighting conditions to minimize the errors due to stray lights or lighting variation at different observation angles. Optical microscopy was performed by the Keyence VH-ZST microscope (20X to

---

[4] Bidirectional reflectance distribution functions

[5] Commission Internationale de l'éclairage
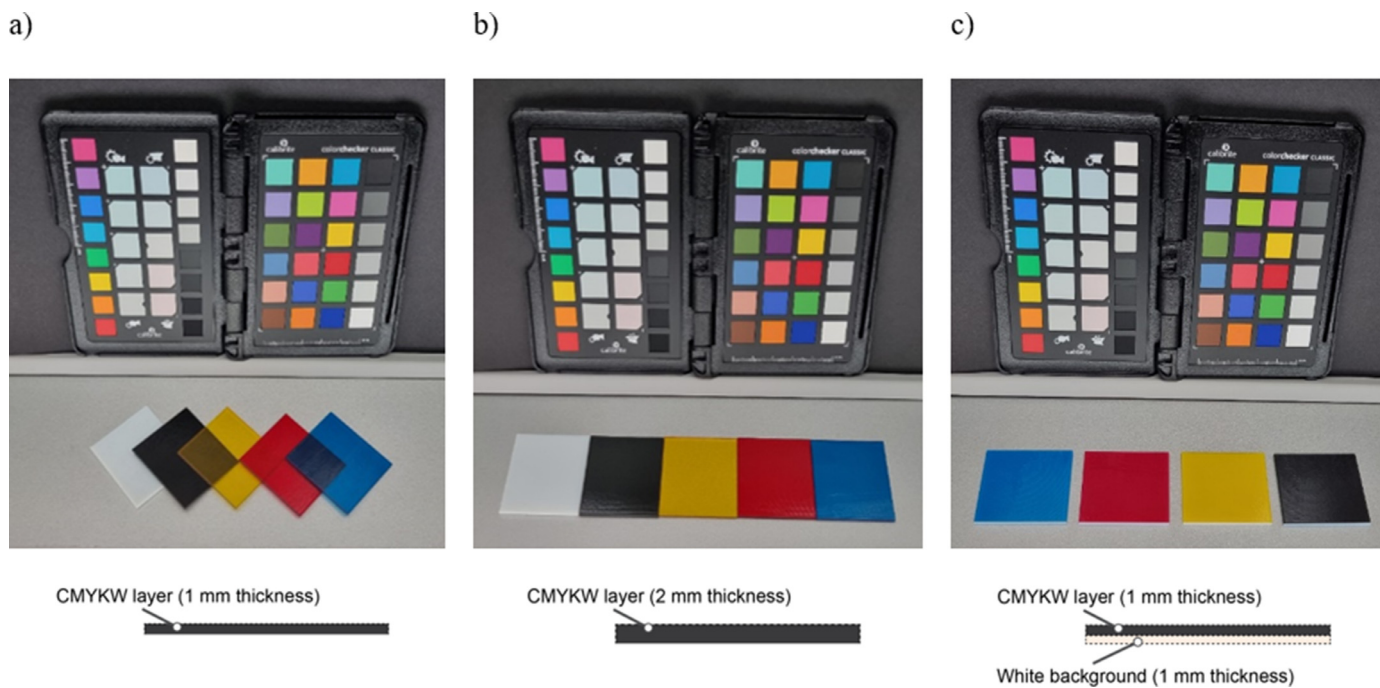[6] Mean color difference from the mean
[7] Root-mean-square error

Fig. 1. CMYKW monolayers (plates) with a thickness of a) 1 mm, b) 2 mm, and c) bilayers of CMYK plate on white background, as observed under D50 daylight illumination.
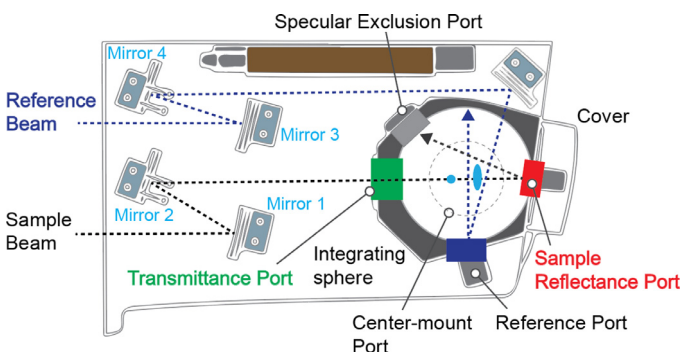

Fig. 2. A top-down schematic representation of the UV/VIS/NIR spectrometer and the measurement geometry.

2000X). An RA-532H surface reflectance analyzer was used to analyze haze and gloss per ASTM D523 – 14. Further, it provided Canon scattering indices C20 and C60 for lighting angles of 20° (ASTM D5767) and 60° (JIS K7374), respectively. The C20 index addresses the DOI[8], and the C60 index refers to IC[9]. Reduction measurement errors were considered by avoiding sites with unusual colors, external particles, stains or dust, and support materials. Data analysis was performed using Origin 2022 (OriginLab) and R statistical software 4.2.1.

3. Results and discussions

3.1. Visual observations

Fig. 3 illustrates how typical PolyJet parts were semi-translucent, hazy, and complex in appearance due to the addition of layering photo resins and the agitation in the manufacturing process. There was a distinction between the appearance of MJT objects under different illumi-

---

[8] Distinctness of the image

[9] Image clarity
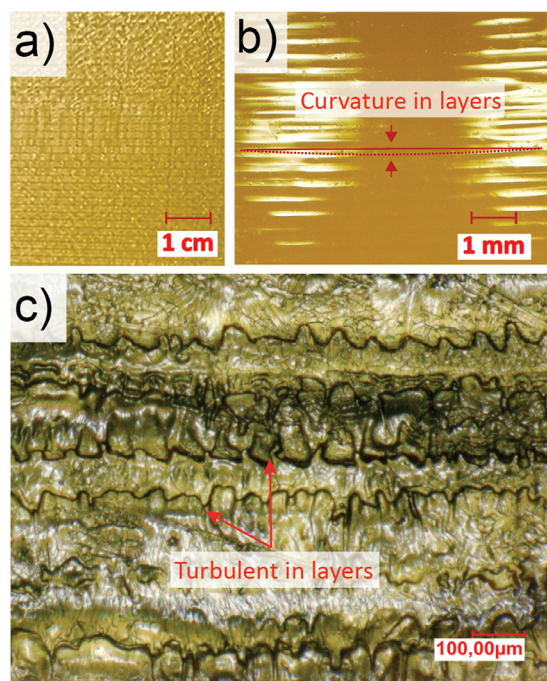
Fig. 3. The polymeric surface of the 3D-printed yellow photo resin as seen through an optical microscope at a) macroscopic 1X, b) macroscopic 10X, and c) microscopic scales.

nations and microscopes. As a result of the disc-shaped build platform (rotary disc), parallel layers (swaths) were not perfectly horizontal, resulting in a slight curvature observable on the surface (Fig. 3b). The added layers were oriented in the same direction as the rotation of the rotary disc. The curvature in layers was primarily determined by the printing speed, as well as the design, which are connected to the UV curing time (the print head) and the rotational speed of the disc. As a
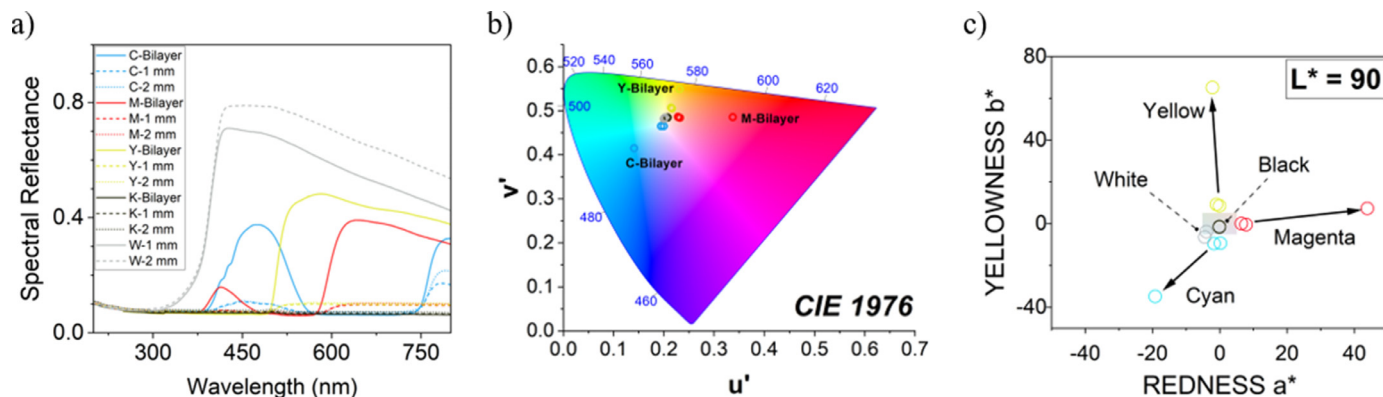
Fig. 4. a) Reflectance, b) the mean hue stimuli in the CIE1976 u', v' chromaticity diagram, and c) redness and yellowness at constant lightness in CIEL*a*b* color space.

Table 1
The color difference results compared with the corresponding bilayer configuration.

Photo resin	Thickness: 1 mm					Thickness: 2 mm				
	MCDM	RMSE	dL	dC	dh	MCDM	RMSE	dL	dC	dh
Cyan	18.83	0.20	9.30	14.71	-4.60	21.12	0.08	8.96	14.98	-7.68
Magenta	19.83	0.12	8.62	17.67	2.56	20.43	0.05	7.96	18.75	1.55
Yellow	38.56	0.09	32.39	20.88	-1.38	38.03	0.08	31.52	21.29	0.32
Black	0.50	0.01	-0.48	-0.14	-0.02	1.52	0.01	-1.51	-0.20	-0.04
White	4.19	0.01	3.63	-1.58	-1.37	-	-	-	-	-

result of typical build vibration during the manufacturing process, the swaths were subject to subsurface turbulence in layers and microscopic inhomogeneity (Fig. 3c).

3.2. Spectrophotometry

Spectrophotometry results, including reflectance, transmittance, and absorbance, indicate that the white background plate for CMYKW plates plays a vital role in visual appearance. As seen in Fig. 4, only using colored plates with 1 mm or 2 mm thickness could not provide the intended color. The spectral reflectance results indicate significantly lower lightness (albedo) due to lower reflectance values (Fig. 4a). Besides, hue stimuli were closely distributed in the middle of the CIE1976 u', v' chromaticity diagram (Fig. 4b). Using white background was crucial to alter the colors to their intended u', v' in GrabCAD, and a* and b* values. It is particularly highlighted for CMY colors as represented by vectors in Fig. 4c.

Table 1 lists the mean color difference of monolayer specimens according to their corresponding bilayer type. According to the results, color reproduction in yellow photo resins was more dependent on the presence of a white background with the highest MCDM of 38.56 for 1 mm thickness and 38.03 for 2 mm thickness. Results were followed by cyan and magenta photo resins, which were mainly affected by color changes associated with chroma (dC) and lightness (dL). The black and white photo resins exhibited the smallest color difference. Furthermore, it was evident that increasing the thickness did not compensate for the color difference.

Table 2 lists the measured CIEL*a*b* values along with their representative color HEX compared to the closest Pantone color codes extracted from GrabCAD. Color variation was inevitable during the reproduction of colors using the J55 3D printer, where the same Pantone code was referred to for the monolayers of cyan and yellow. In the manufacturing design, even 1 mm monolayers and bilayers of black photo resin follow the same Pantone code. A darker specimen with less lightness, particularly for monolayer specimens, suggests that studying color appearance alone is insufficient for the optical assessment of MJT products. Translucency, gloss, and scattering are essential factors to accurately re-

produce an appearance to fulfill hard proofing in the appearance of 3D printing.

Fig. 5 shows that using a white background significantly decreases transmission and increases the absorbance of light through the specimens. Yellow, cyan, and magenta photo resins showed a similar trend in reflectance compared to black and white resins, which appeared opaquer. While the 1 mm thickness exhibited considerably greater transparency than the 2 mm, the role of the white background was the dominant factor in translucency and appearance reproduction.

3.3. Gloss appearance

To characterize gloss nuances, distinct aspects of gloss appearance have been compared in Fig. 6. This includes specular gloss, haze, and scattering results of C20 and C60 derived from BRDF. Compared to monolayer specimens, adding a white background plate results in generally increased gloss and haze, but had no significant influence on the sublayer scattering. Haze in reflection indicates a cloudy or milky appearance caused by light scattering [34]. As part of surface quality assessment, haze is considered an appearance attribute that reduces the quality of the appearance because of imperfections, including surface texture. High haze occurs around reflections of light sources on high-gloss and high-scattering (C20 and C60) surfaces due to image diffusion.

The results show the gloss results of the same samples measured vertically (Fig. 6a) were generally higher than that measured horizontally (Fig. 6b). In addition, results were more correlated depending on the photo resin used, as indicated by the stronger fitting of the mean (red lines in Fig. 6a and b) for vertical gloss ($R^2 = 0.46$) and associated haze ($R^2 = 0.50$) measurements. According to Spearman's rank correlation coefficient (ρ) in Fig. 6c, robust correlations were observed between measurement direction and studied variables, including gloss ($\rho = 0.59$), and the haze and scattering results ($\rho = 0.87$). Therefore, surface reflectance analysis was significantly affected by the measurement direction. Furthermore, gloss showed a correlation of $\rho = 0.50$ with the sample type.

In the vertical direction, higher R^2 values indicate a strong correlation in the data, suggesting that the type of photo resins plays a less

Table 2
Measured color compared to the corresponding Pantone color at the design level.

| Digital material	Type	Color measurement					Pantone Solid Coated					
		L^*	a^*	b^*	HEX		Code	L^*	a^*	b^*	HEX	
Cyan	Bilayer	43.67	-19.23	-34.73	0073A0		641 C	41.18	-30.48	-38.07	00719F	
	1 mm	32.84	-1.76	-9.45	424F5C		7540 C	33.71	-1.57	-3.98	495055	
	2 mm	33.27	0.13	-9.26	464F5D		7540 C	33.71	-1.57	-3.98	495055	
Magenta	Bilayer	42.23	43.81	7.34	A64159		7419 C	44.77	42.90	6.77	AC4960	
	1 mm	32.04	7.80	-0.38	57474C		438 C	30.87	11.34	-0.28	5A4249	
	2 mm	32.86	6.40	0.16	584A4D		2335 C	34.08	5.60	4.57	5C4D49	
Yellow	Bilayer	70.72	-2.23	65.20	C9AB2A		7752 C	70.86	3.66	66.63	D2A827	
	1 mm	37.08	-1.02	9.27	5C5748		411 C	35.93	4.72	2.72	5E5250	
	2 mm	37.81	-0.14	8.59	5E594B		411 C	35.93	4.72	2.72	5E5250	
Black	Bilayer	30.92	-0.16	-1.32	48494B		2336 C	31.98	0.66	1.41	4D4B49	
	1 mm	31.53	-0.16	-1.47	494A4C		2336 C	31.98	0.66	1.41	4D4B49	
	2 mm	32.83	-0.16	-1.53	4C4D50		7540 C	33.71	-1.57	-3.98	495055	
White	Bilayer	83.24	-4.50	-6.31	C0D2DB		5455 C	82.44	-3.63	-9.38	BCD0DE	
	1 mm	88.82	-4.02	-3.72	D3E2E6		621 C	88.31	-5.84	0.03	D2E1DD	
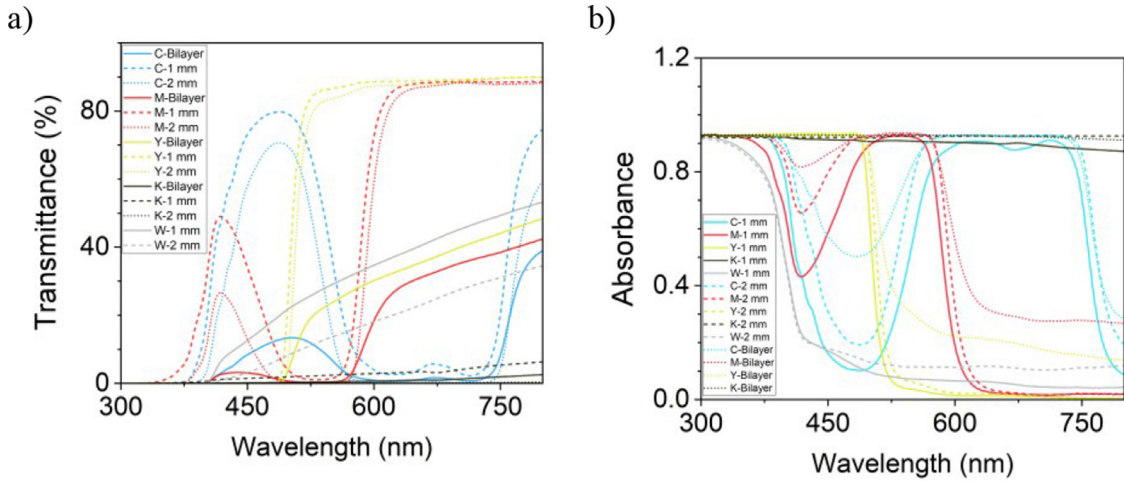
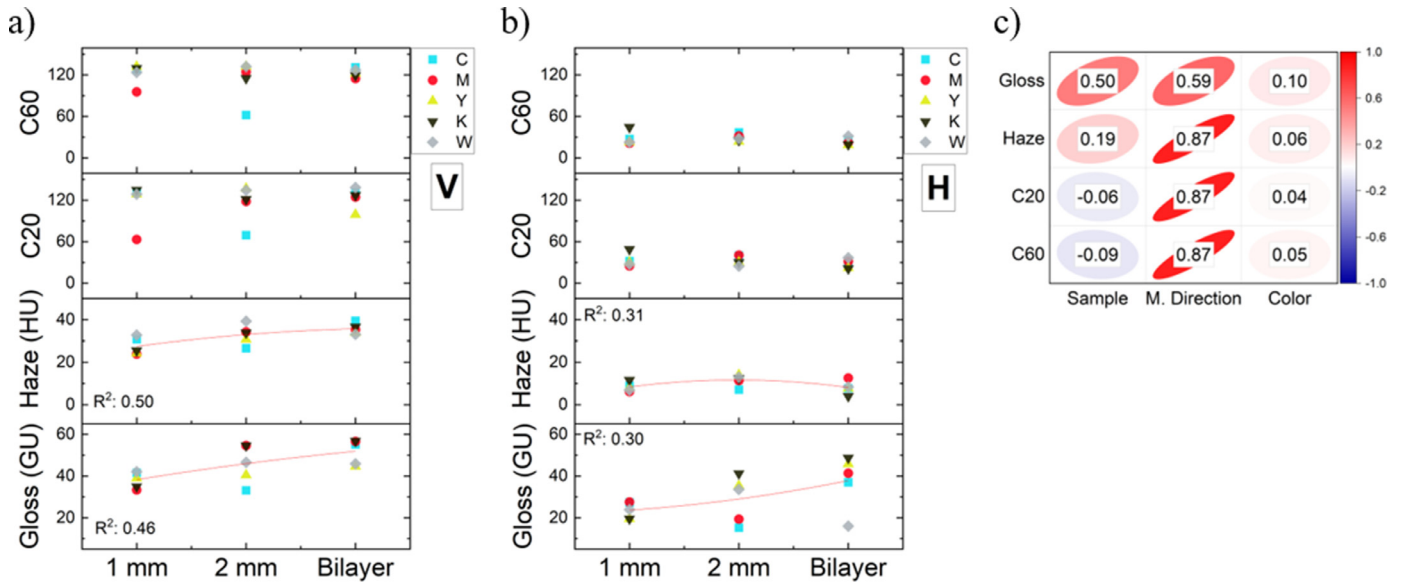**Fig. 5.** a) Transmittance and b) absorbance in the visible spectrum.

Fig. 6. Gloss nuances in a) vertical and b) horizontal measurement directions, and c) Spearman rank correlation coefficients.

significant role in surface reflectance variations. This can be explained by considering the more significant effect of $\vec{m}$, microfacets normals (Fig. 7), facing toward the measurement direction in the vertical mode. According to Fresnel's equation [35], the $f_{r,m}$ term explains the reflectance from a smooth microfacet in translucent objects in the BSDF[10]:

$$f_{r,m}\left(x_m, \vec{\omega}_i, \vec{\omega}_o\right) = F\left(\vec{m}, \vec{\omega}_i, \frac{n_t}{n_i}\right) \frac{\delta\left(\vec{\omega}_o - \vec{\omega}_s\right)}{\cos \theta_i} \quad (4)$$

where x_m is the microfacet surface point, $\vec{\omega}_i$, $\vec{\omega}_s$ and $\vec{\omega}_o$ are the unit vectors for illumination, scattering, and observation of light. F is the expansion of Maxwell's equations along the surface using Fourier transformation. n_t and n_i are the transmission and illumination normals. δ is the Dirac delta function and θ_i is the illumination angle relative to the surface normal ($\vec{n}$).

The macroscopic BSDF is a function that includes both reflectance (BRDF) and transmittance (BTDF[11]). In this case, the light is incident on and emerges from the same macroscopic surface [36]. Accordingly, smoother BRDFs were captured for vertical measurement compared to
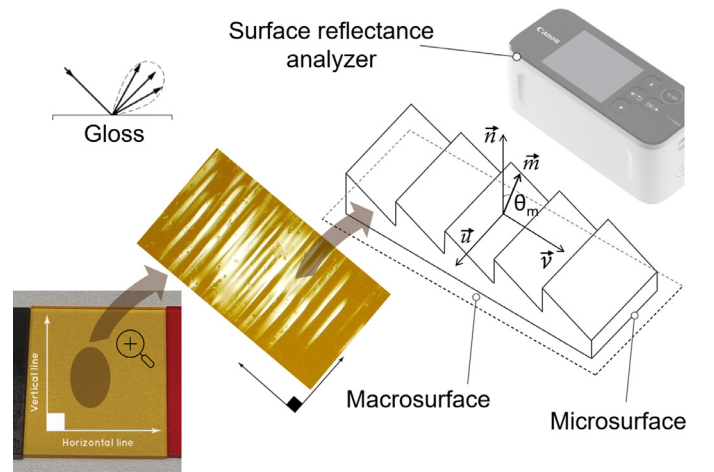

Fig. 7. Gloss measurement for structured surfaces in additive manufacturing.

---

[10] Bidirectional scattering distribution function
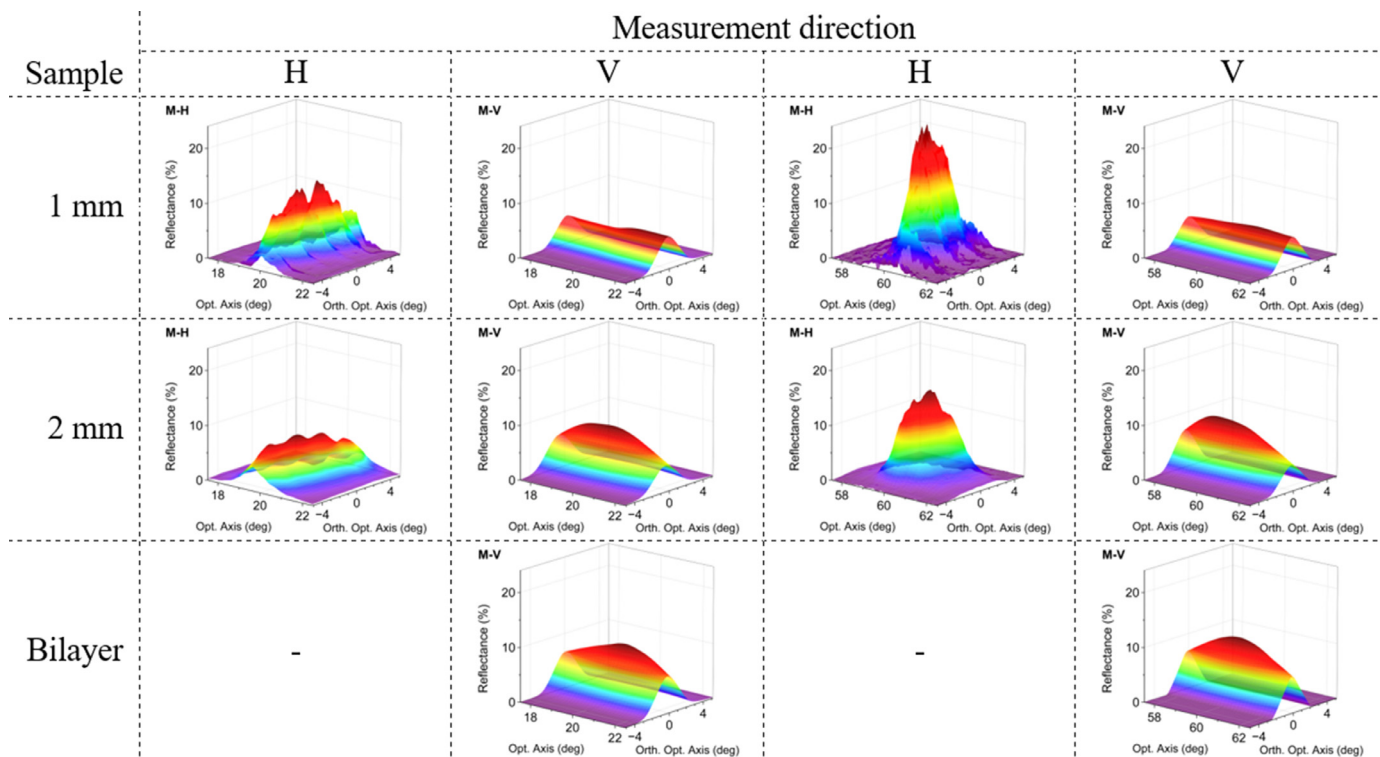[11] Bidirectional transmittance distribution function

Fig. 8. BRDF representations for magenta resin at specular angles of 20° and 60°.

the horizontal direction (Fig. 8). The mixture of curvature on the surface shown in Fig. 3b which can affect the direction of microfacet normals provides an insight into the reason behind these perturbed BRDF graphs. Supplementary BRDF data for specular gloss measurements are available in Appendix A.

3.4. Visual texture mapping

Illustrations of texture mapping on spherical 3D models using surface textural maps are shown in Fig. 9. Photo resins of cyan and magenta exhibited notable parallel horizontal swathes fabricated in the manufacturing process. The swath patterns were also apparent for yellow bilayer samples. However, black photo resins did not show the same texture characteristics. The bilayer specimens for the CMY photo resins exhibited significantly different appearances with more specular reflection, particularly for the color attribute. However, in black materials, the role of the white background film was less apparent. Table 2 confirms this behavior for monolayers of black resins of 1 mm and bilayers of black resins of 2 mm with more diffuse reflection. Results for CMY photo resins also suggest a higher glossiness and less transparency than monolayers, which is consistent with the results of the spectrophotometry and gloss measurements. Because of the high exposure surface of the white photo resins, it was impossible to generate rendered spheres properly for this material. Although yellow specimens experienced the same problem at lower significance, particularly monolayer samples, they rendered the results. Supplementary results for texture mapping, including surface displacement and normal maps, are available in Appendix B.

4. Conclusions

This study aimed to provide insight into the role of bilayer structure in material jetting appearance reproduction. A PolyJet printer was used to deposit photo resins in CMYKW colors in monolayers varying in thickness, as well as bilayers using a white background plate. According to the findings of this study:
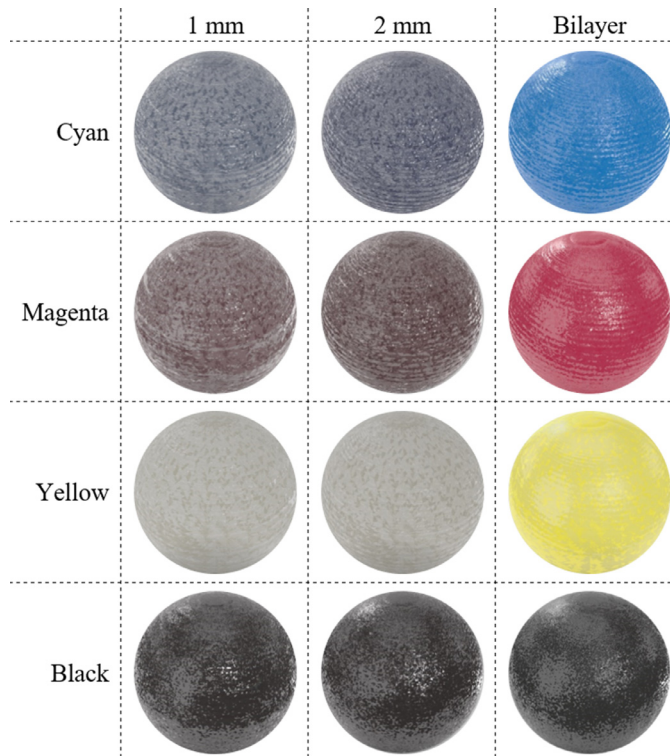

Fig. 9. A series of spheres rendered in different texture levels.

- Microscopical observations revealed a distinction between the appearance of MJT objects and their visual complexity under different illuminations and microscopic scales. As a result of layer-by-layer rotational printing, vibrations of the rotary disc as the build plat-

form, and translucency of photo resins, the texture, and appearance showed more subsurface turbulence in layers and microscopic inhomogeneities.

- Spectrophotometry revealed that the lack of a white background plate led to an increase in transparency and a decrease in albedo and color fidelity.
- Using only monolayer CMYKW resins resulted in significant deviations in CIEL*a*b* and CIE1976 u', v' from the Pantone color matching scheme, with more significant deviations in chroma and lightness.
- The increase in absorbance due to doubling the thickness of monolayer samples did not compensate for losing albedo and higher reflectance because of the lack of white background plates in the monolayer samples.
- The gloss perception was characterized by a monolayer/bilayer structure similar to that seen in transmittance conditions. Color and texture of the reflective surface changed according to the embedding illumination. Higher gloss and haze were recorded for bilayer specimens compared to monolayers.
- The white background had a greater impact on color, translucency, and scattering than gloss and haze. Vertical measurements resulted in higher values of gloss, haze, and scattering compared to the horizontal measurements.
- In monolayer structures, cyan, magenta, and yellow photo resins had significantly different appearances, as shown in rendered spherical 3D models. MJT photo resins exhibited high transparency, specular reflections, and non-uniform albedo due to textured surfaces.

In summary, assessing the appearance attributes of detailed properties on MJT surfaces using only color and gloss in a fixed measurement direction is challenging due to the full-color capability of this AM method. Future research needs to focus on detailed BRDF and BTDF analysis using gonio-spectrophotometers to reproduce accurate appearances.

Declaration of Competing Interest

The authors declare the following financial interests/personal relationships which may be considered as potential competing interests:

Ali Payami Golhin reports financial support, and article publishing charges were provided by Horizon 2020 (EU) ApPEARS-ITN project [grant No. 814158].

CRediT authorship contribution statement

Ali Payami Golhin: Conceptualization, Methodology, Investigation, Data curation, Formal analysis, Visualization, Writing – original draft, Writing – review & editing. **Are Strandlie:** Writing – review & editing, Supervision, Project administration, Funding acquisition.

Data availability

The main part of the raw/processed data required to reproduce these findings is available at https://doi.org/10.5281/zenodo.7580082.

Acknowledgments

Supplementary materials

Supplementary material associated with this article can be found, in the online version, at doi:10.1016/j.optlaseng.2023.107632.

References

[1] Msallem B, Sharma N, Cao S, et al. Evaluation of the dimensional accuracy of 3D-printed anatomical mandibular models using FFF, SLA, SLS, MJ, and BJ printing technology. 2020;9:https://doi.org/10.3390/jcm9030817

[2] Baharnezhad S, Golhin A. In-situ measurement and finite element simulation of thermo-mechanical properties of AA 6063 aluminum alloy for MIG weldment. 2017;32:https://doi.org/10.18720/MPM.3222017_15

[3] Ai Y, Liu X, Huang Y, et al. Numerical analysis of the influence of molten pool instability on the weld formation during the high speed fiber laser welding. 2020;160:120103. https://doi.org/10.1016/j.ijheatmasstransfer.2020.120103

[4] Ai Y, Yu L, Huang Y, et al. The investigation of molten pool dynamic behaviors during the "∞" shaped oscillating laser welding of aluminum alloy. 2022;173:107350. https://doi.org/10.1016/j.ijthermalsci.2021.107350

[5] Dorweiler B, Baqué PE, Chaban R, et al. Quality control in 3D printing: accuracy analysis of 3D-printed models of patient-specific anatomy. 2021;14:1-13. https://doi.org/10.3390/ma14041021

[6] Di Nicolantonio M, Rossi E, Stella P. Generative design for printable mass customization jewelry products, E. Rossi, T. Alexander, and. M. Di Nicolantonio, Editors., Springer Verlag 2020; p. 143-152. https://doi.org/10.1007/978-3-030-20216-3_14

[7] Ulu FI, Mohan RV. Voxel and stereolithographic digital design framework in additive manufacturing: effects in a PolyJet printing process and relevant digital solutions. Prog. Addit. Manuf. 2021;6:653–62. doi:10.1007/s40964-021-00186-2.

[8] Golhin AP, Sole AS, Strandlie A. Color appearance in rotational material jetting. Int. J. Adv. Manuf. Technol. 2023;124:1183–98. doi:10.1007/s00170-022-10536-1.

[9] Payami Golhin A, Strandlie A, John Green P. The influence of wedge angle, feedstock color, and infill density on the color difference of FDM objects. J. Imag. Sci. Technol. 2021;65:1–15. doi:10.2352/J.ImagingSci.Technol.2021.65.5.050408.

[10] Zheng Y, Zhang X, Wang SD, et al. Similarity evaluation of topography measurement results by different optical metrology technologies for additive manufactured parts. Opt. Lasers Eng. 2020;126:7. doi:10.1016/j.optlaseng.2019.105920.

[11] Choudhury AKR. Principles of colour and appearance measurement: Object appearance, colour perception and instrumental measurement. Elsevier; 2014.

[12] Pointer MR. Measuring visual appearance-a framework of the future. Project 2.3 measurement of appearance. 2003;

[13] Hunt RWG, Pointer MR. Measuring colour. John Wiley & Sons; 2011.

[14] Payami Golhin A. Generation of micro-and nano-textured surfaces. Eur. Commission: Brussels 2021:1–6. doi:10.5281/zenodo.7293168.

[15] Yuan J, Chen G, Li H, et al. Accurate and computational: a review of color reproduction in full-color 3D printing. Mater. Des. 2021;209:1–17. doi:10.1016/j.matdes.2021.109943.

[16] Wei X, Bhardwaj A, Zeng L, et al. Prediction and compensation of color deviation by response surface methodology for polyjet 3d printing. J. Manuf. Mater. Process. 2021;5. doi:10.3390/jmmp5040131.

[17] Zeng J, Deng H, Zhu Y, et al. Lenticular objects: 3D printed objects with lenticular lens surfaces that can change their appearance depending on the viewpoint. In: UIST 2021 - Proceedings of the 34th Annual ACM Symposium on User Interface Software and Technology; 2021.

[18] Sohaib A, Amano K, Xiao KD, et al. Colour quality of facial prostheses in additive manufacturing. Int. J. Adv. Manuf. Technol. 2018;96:881–94. doi:10.1007/s00170-017-1480-x.

[19] Urban P. Graphical 3D printing: challenges, solutions and applications. London Imaging Meeting. Society for Imaging Science and Technology, 1; 2020. doi:102352/issn2694-118X2020LIM-35.

[20] Elkhuizen W, Essers T, Song Y, et al. Gloss, color, and topography scanning for reproducing a Painting's appearance using 3D printing. 2019;12:https://doi.org/10.1145/3317949

[21] Zheng L, Li C, Yang S. Analysis of color gamut in color 3D printing. 2020;600:148-155. https://doi.org/10.1007/978-981-15-1864-5_21

[22] Cheng YL, Huang KC. Preparation and characterization of color photocurable resins for full-color material jetting additive manufacturing. Polymers (Basel) 2020;12:650. doi:10.3390/polym12030650.

[23] Wei X, Zeng L, Pei Z. Experimental investigation of polyjet 3D printing process: effects of finish type and material color on color appearance. In: ASME International Mechanical Engineering Congress and Exposition (IMECE); 2019.

[24] Acosta-Vélez GF, Zhu TZ, Linsley CS, et al. Photocurable poly(ethylene glycol) as a bioink for the inkjet 3D pharming of hydrophobic drugs. Int. J. Pharm. 2018;546:145–53. doi:10.1016/j.ijpharm.2018.04.056.

[25] Payami Golhin A, Srivastava C, Tingstad JF, et al. Additive manufacturing of multilayered polymer composites: durability assessment. In: Proceedings of the 20th European Conference on Composite Materials-Composites Meet Sustainability, 1-6. EPFL Lausanne, Composite Construction Laboratory Switzerland; 2022.

[26] Payami Golhin A, Srivastava C, Strandlie A, et al. Effects of accelerated aging on the appearance and mechanical performance of materials jetting products. Materials & Design 2023;228:111863. doi:10.1016/j.matdes.2023.111863.

[27] Hong W, Yuan Z, Chen X. Structural color materials for optical anticounterfeiting. 2020;16:https://doi.org/10.1002/smll.201907626

[28] Nam SH, Park J, Jeon S. Rapid and large-scale fabrication of full color woodpile photonic crystals via interference from a conformal multilevel phase mask. Adv. Funct. Mater. 2019;29:10. doi:10.1002/adfm.201904971.

[29] Hsu WC, Peng TY, Kang CM, et al. Evaluating the effect of different polymer and composite abutments on the color accuracy of multilayer Pre-colored Zirconia Polycrystal dental prosthesis. 2022;14:doi:10.3390/polym14122325.

[30] Egorov V, Gulzar U, Zhang Y, et al. Evolution of 3D printing methods and materials for electrochemical energy storage. 2020;32:doi:10.1002/adma.202000556.

[31] Tee YL, Peng C, Pille P, et al. PolyJet 3D printing of composite materials: experimental and modelling approach. JOM 2020;72:1105–17. doi:10.1007/s11837-020-04014-w.

[32] Stratasys. Vero: realistic, multi-color prototypes in less time, in Stratasys Datasheet. 2022; p. 1-4.

[33] Westland S, Ripamonti C, Cheung V. Computational colour science using MATLAB. John Wiley & Sons; 2012.

[34] Astm. Standard terminology of appearance, A. E284-17, Editor., ASTM International West Conshohocken, PA 2017; p. 1-25. doi:10.1520/E0284-17.

[35] Bell EE. Optical Constants and their Measurement. In: Genzel L, editor. Light and Matter Ia /Licht und Materie Ia. Berlin, Heidelberg: Springer Berlin Heidelberg; 1967. p. 1–58. Editor.

[36] Frisvad JR, Jensen SA, Madsen JS, et al. Survey of models for acquiring the optical properties of translucent materials. Computer graphics forum, 2. Wiley Online Library; 2020. doi:10.1111/cgf.14023.

Ali Payami Golhin is a Ph.D. candidate at NTNU - Norwegian University of Science and Technology. He has research experience in the optical properties of structured surfaces as an ApPEARS fellow, which is funded by the Marie Sklodowska-Curie Actions under the Horizon Europe program. He has research experience in additive manufacturing, optical measurement, tribology, and surface science.

Are Strandlie is a Professor of Physics at NTNU - Norwegian University of Science and Technology. His main research interests are data analysis methods for high-energy physics experiments and numerical methods for material physics. Recently, an increasing interest has emerged within cross-disciplinary topics, such as the link between appearance and material properties.